Applied Surface Science 447 (2018) 355–362

Contents lists available at ScienceDirect

Applied Surface Science

journal homepage: www.elsevier.com/locate/apsusc

Decoupling the effects of surface texture and chemistry on the wetting of metallic glasses

Molla Hasan [a,*], Juliusz Warzywoda [b], Golden Kumar [a]

[a] Department of Mechanical Engineering, Texas Tech University, TX 79409, USA
[b] Materials Characterization Center, Whitacre College of Engineering, Texas Tech University, TX 79409, USA

ARTICLE INFO

Article history:
Received 1 November 2017
Revised 16 February 2018
Accepted 24 March 2018
Available online 27 March 2018

Keywords:
Metallic glasses
Thermoplastic forming
Demolding
Wetting
Superhydrophobic

ABSTRACT

We report the effects of surface patterning on the wetting of $Pt_{57.5}Cu_{14.7}Ni_{5.3}P_{22.5}$ and $Pd_{43}Cu_{27}Ni_{10}P_{20}$ metallic glasses. To maintain the integrity of surface chemistry of the metallic glasses, we optimize thermoplastic patterning protocol and use chemical-free demolding. Our results show that single-scale surface microstructures can render inherently hydrophilic $Pt_{57.5}Cu_{14.7}Ni_{5.3}P_{22.5}$ metallic glass hydrophobic when its chemical state is preserved. We also observe that because of oxidation, $Pd_{43}Cu_{27}Ni_{10}P_{20}$ metallic glass remains hydrophilic regardless of its surface topography, though its wettability evolves (i.e. decreases) with time due to airborne contamination. These results suggest that to draw an unambiguous conclusion about the role of surface texture, concomitant changes in surface chemistry must be avoided.

1. Introduction

Significant research has been conducted on wetting to better understand and control the solid-liquid interaction for emerging applications. Applications of wetting range from household self-cleaning surfaces to advanced fields, including metallic parts with enhanced corrosion resistance [1], transparent [2] and anti-reflective coatings [3], anti-freezing surfaces [4], smart filters for oil-water separation [5], and drag-reducing topographies [6]. Wetting is controlled by the combined effects of surface chemistry and topography. Low surface energy materials [e.g. Teflon, PDMS (Polydimethylsiloxane), and PMMA (poly(methylmethacrylate))] are typically hydrophobic. The role of surface texture in wetting has not been conclusively determined, however, especially in high surface energy materials such as metals. According to the Wenzel model, texture alone cannot induce hydrophobicity in metals because it amplifies the intrinsic wetting behavior, i.e. hydrophilic materials (e.g. metals and semiconductors) become more hydrophilic [7–10] and hydrophobic materials tend to become superhydrophobic with increasing roughness [10–12]. Although the Wenzel model has been well established for low-energy materials (e.g. polymers), its applicability to metals and semiconductors remains in question. Numerous studies have demonstrated the manifestation of the Wenzel model by showing roughness induced increase in the hydrophilicity of metals and semiconductors [7,9,13]. Several other studies have challenged Wenzel's hypothesis [14–18], however, showing that hydrophilic metals can be made superhydrophobic through topographical engineering alone. The major challenges to overcoming this ambiguity in metallic materials are: (1) the lack of methods for systematically patterning surfaces at multiple length scales and (2) the inability to prevent changes in surface chemistry during the patterning processes. The finite grain sizes of crystalline metals limit the fabrication of feature with sub-micron length scales [19]. A few methods have recently been introduced to engineer the surface topography of metals, including femto second laser irradiation [15,16,20], electrochemistry [21], chemical etching [22], and sandblasting [23]. These methods, however, are either unable to produce controllable structures or simultaneously alter the surface chemistry, potentially overriding the topography-wetting correlation. To quantify the effect of topography on wetting, systematically tunable surfaces are needed to control the fraction of solid-liquid and solid-air interface. To discern the true effect of texture, moreover, the chemical composition and the structural state of metals must be preserved during patterning.

Metallic glasses (MGs) have emerged as model materials for studying the effects of topography on surface properties owing to their isotropic and homogeneous structure [24,25] and ease in patterning ability through thermoplastic techniques [26–28]. Recently, MGs have also been used for wetting studies [29–35]. Thermoplastically patterned $Pd_{40}Cu_{30}Ni_{10}P_{20}$ and $Zr_{35}Ti_{30}Be_{26.75}Cu_{8.25}$

* Corresponding author at: Box 41021, Lubbock, TX 79409, USA.
E-mail address: molla.hasan.ttu@gmail.com (M. Hasan).

https://doi.org/10.1016/j.apsusc.2018.03.205
0169-4332/

MGs showed a combination of relatively high contact angles (CAs) and adhesion with water [29–31]. These studies did not conclusively determine the effect of surface roughness on wetting, however, because the MGs studied were susceptible to oxidation during thermoplastic processing. In addition to oxidation, the chemical etchant used to separate MGs from the mold after thermoplastic patterning can also change the surface composition of MGs. For these reasons, to draw unambiguous conclusions about the topography-wetting correlation, chemical state of MGs should be characterized before and after thermoplastic patterning. Minimizing these uncertainties is the main objective of this work. First, we selected $Pt_{57.5}Cu_{14.7}Ni_{5.3}P_{22.5}$ (Pt-MG) for its high oxidation resistance. Second, to understand the effects of surface composition and topography on wetting, we characterized the chemical state and wetting of the MG at different stages of thermoplastic processing. To compare the role of topography in the wetting of other MGs, we extended the systematic approach to $Pd_{43}Cu_{27}Ni_{10}P_{20}$ (Pd-MG).

2. Experimental

2.1. Materials

Ingots of $Pt_{57.5}Cu_{14.7}Ni_{5.3}P_{22.5}$ (at.%) and $Pd_{43}Cu_{27}Ni_{10}P_{20}$ (at.%) alloys were made by melting the elemental mixtures in vacuum-sealed quartz tubes. The ingots were melted twice to achieve compositional homogeneity. Subsequently, the ingots were fluxed with boron oxide (B_2O_3) under high vacuum to improve the glass forming ability of alloys by reducing the heterogeneous nucleation sites. To produce cylindrical MG specimens of 2 mm diameters, the ingots were melted and water quenched in thin-walled quartz tubes. Silicon templates with micro-features were prepared using deep-reactive-ion-etching (DRIE). Silicon templates were covered with a thin oxide layer. Commercially available anodic aluminum oxide (AAO) was used as template for the nano-scale features.

2.2. Thermoplastic forming

Thermoplastic forming (TPF) was used to systematically pattern Pt-MG and Pd-MG for wetting studies. TPF utilizes the softening behavior of MG supercooled liquids. The supercooled liquid refers to the metastable state of MGs between the glass transition temperature (T_g) and the crystallization temperature (T_x). TPF has been widely used to pattern MGs, and excellent reviews are available for further reading [36,37]. Although all embossing experiments were performed at the same temperature, the nano-scale embossing required a higher pressure to achieve the same aspect-ratio due to capillary pressure [26]. The wetting of Pt-MG with silicon and alumina templates is comparable due to the presence of silicon dioxide layer on silicon [38]. Both nano- and micro-pillars of MGs exhibited similar tip shapes (convex) due to parabolic velocity profile during thermoplastic molding. The embossing pressures for the micro- and the nano-patterned MGs were 10 MPa and 50 MPa, respectively. The MG and the mold were mechanically interlocked after thermoplastic embossing due to thermal expansion mismatch [39]. For this reason, demolding was carried out by etching the mold in 2 M KOH solution at 350 K. The MG was then rinsed with deionized water to get rid of any residue and dried with argon gas prior to being used in the wetting experiments.

2.3. Surface characterization

The surface wettability of MGs was measured using the sessile drop method, in which 2 µl droplets of deionized water were dispensed onto the surfaces of MGs using a micro-pipette and the static contact angles (CAs) were measured with a goniometer (model Wet Scientific). The surface morphologies of MGs were characterized using a Hitachi S4300 scanning electron microscope (SEM)). The surface chemical states of MGs were characterized using a PHI 5000 VersaProbe X-ray photoelectron spectrometer (XPS).

3. Results and discussion

3.1. The wetting of Pt-MG

To understand the effect of surface texture on wetting, Pt-MG samples were thermoplastically patterned with three different topographies: flat, nano-patterned, and micro-patterned (Fig. 1). Silicon and AAO were used as molds for the micro- and the nano-patterning, respectively. The CA of the flat Pt-MG was 55°, but the patterning made the samples more hydrophilic (Fig. 1b), as is evident from the lower CAs of micro- (5°) and nano-patterned (14°) samples. This increased hydrophilicity can be explained by the Wenzel model, which relates contact angle to surface roughness as follows [40]:

$$\cos\theta^* = r\cos\theta_Y, \quad (1)$$

where θ^* is the apparent contact angle, r is the roughness factor (the ratio of the actual surface area to the apparent surface area), and θ_Y is the Young contact angle (also known as the "intrinsic contact angle" of the flat surface). According to the Wenzel equation (Eq. (1)), the possible causes for the increase in the hydrophilicity (decrease in θ^*) of the textured MG samples are: (1) an increase in surface roughness (r) due to patterning and/or (2) a decrease in intrinsic contact angle (θ_Y) due to oxidation during thermoplastic embossing and/or wet etching.

Since similar surface patterns have been reported to facilitate the hydrophobicity in other MGs [29–31], it is important to determine whether the surface chemistry of Pt-MG changes during thermoplastic forming and wet etching. To this end, XPS was used to analyze the surface chemistry of Pt-MG at different stages of thermoplastic processing. Four disc-shaped unpatterned samples of Pt-MG were prepared to mimic the different stages of the thermoplastic embossing experiment. The first sample was prepared from the as-cast Pt-MG and was used as a reference. Two samples were prepared via thermoplastic embossing at 533 K and 553 K, processing temperatures typically used for Pt-MG. Another sample was thermoplastically embossed at 533 K and exposed to KOH for two hours at 350 K. These four samples capture the different stages experienced by Pt-MG during thermoplastic patterning (Fig. 2). Fig. 3 shows the high-resolution XPS spectra of the Platinum (Pt) 4f, Copper (Cu) 2p, Nickel (Ni) 2p, and Phosphorus (P) 2p of the Pt-MG in the as-cast state, after thermoplastic forming (at 533 K and 553 K), and after KOH exposure. The binding energies (BEs) and kinetic energies (KEs) of the XPS spectra were charge-corrected using the C 1s peak of adventitious carbon (BE = 284.8 eV). The states of the surface elements were identified by analyzing the number of peak components and their position/shape in the deconvoluted XPS spectrum. The Pt 4f peaks of all four samples had asymmetric shapes (Fig. 3a) and the BEs of the Pt $4f_{7/2}$ component ranged from 71.0 eV to 71.6 eV (Table 1). These results agree with the data provided in the literature for the peak shapes in the Pt 4f region and the Pt $4f_{7/2}$ BE for Pt metal [41,42]. This suggests that the state of the Pt in Pt-MG is unaffected by thermoplastic processing and exposure to KOH. For all four samples, the absence of satellite features in the Cu 2p region (Fig. 3b), the BE values of the Cu $2p_{3/2}$ component (932.0 – 932.2 eV, Table 1), and KE values of the Cu LMM peak (918.4 – 918.7 eV, Table 1) are consistent with the literature on Cu metal. This indicates that Cu also retains its

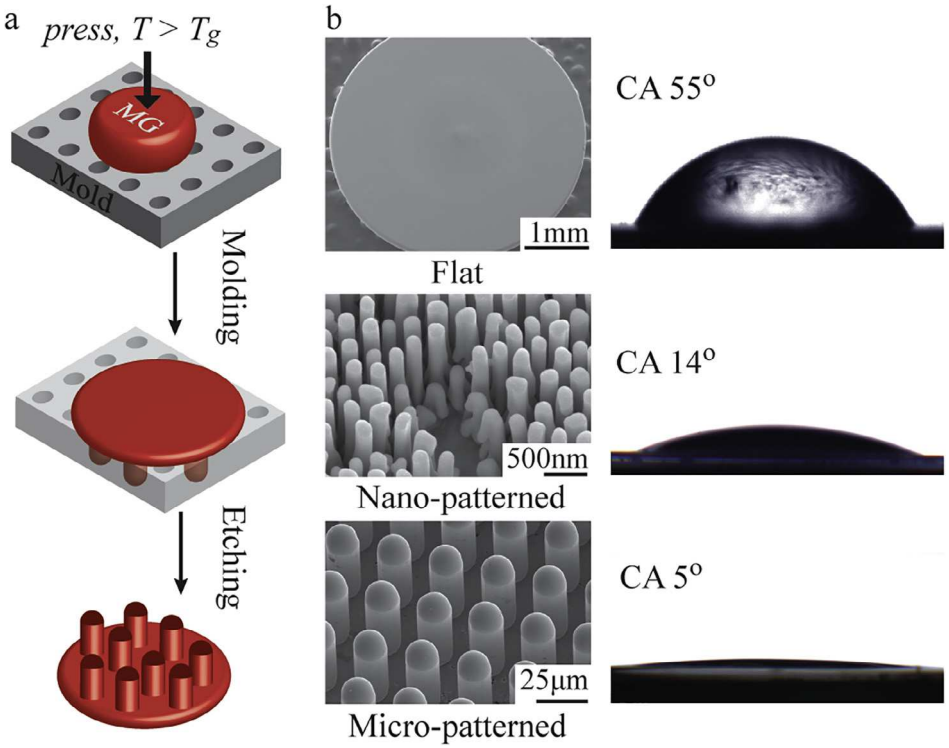

Fig. 1. (a) Schematic illustration of the surface patterning of MGs through thermoplastic embossing. (b) SEM images of flat, nano-patterned and micro-patterned Pt-MGs (left column) and their corresponding CA measurements (right column).

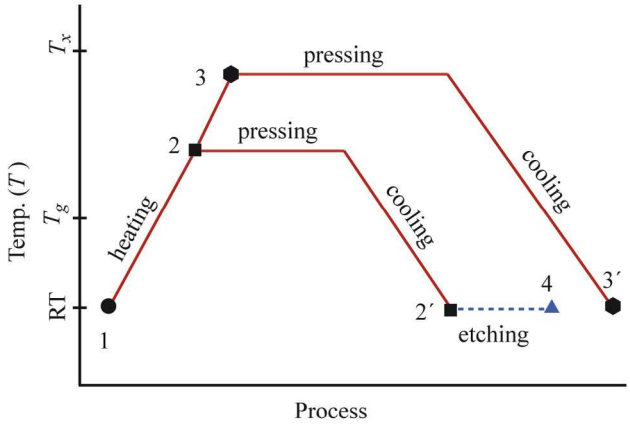

Fig. 2. The different stages of the thermoplastic processing of Pt-MG. As-cast sample was in stage 1 and was not subjected to any heating. The sample prepared in process 1-3-3′ experienced higher temperatures than did the sample prepared in process 1-2-2′. To study the effect of temperature, two samples were prepared at two different temperatures: 533 K and 553 K. The sample prepared in process 1-2-2′-4 underwent heating and etching (KOH) and was used to observe the effect of KOH.

initial metallic form throughout thermoplastic processing and KOH exposure [43,44]. In contrast, the positions and numbers of the XPS peaks in the Ni 2p spectra of the four samples differed significantly (Fig. 3c). The asymmetric peaks (Fig. 3c) and the BE values of the Ni $2p_{3/2}$ component (852.2 – 852.7 eV, Table 1) for the as-cast and thermoplastically formed (at 533 K) samples match the data in the literature for Ni metal [42,45–47]. The Ni 2p spectra of the sample thermoplastically formed at 553 K and the sample exposed to KOH, however, show additional features apart from peaks characteristic of Ni metal (Ni $2p_{3/2}$ BE = 852.6 – 852.7 eV, Table 1). These additional features suggest that the chemical state of Ni on the surface of these two samples has been modified during

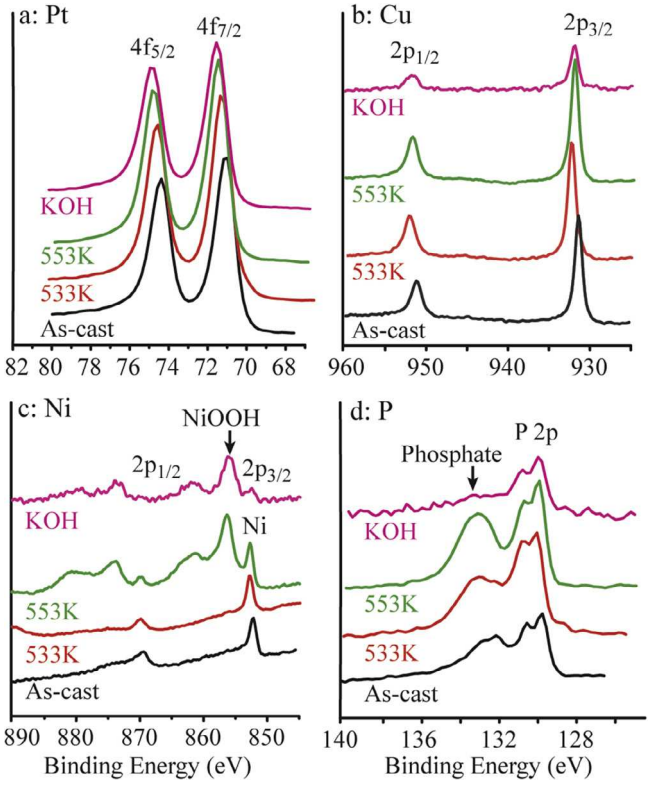

Fig. 3. The XPS spectra of Pt-MG (Pt, Cu, Ni, and P) at four different processing states: as-cast, thermoplastic processing at 533 K and 553 K, and thermoplastic processing at 533 K and after being treated with KOH.

processing. The shape and the BE of the additional Ni $2p_{3/2}$ component (856.1 – 856.2 eV, Table 1) and the satellite features in both samples (Fig. 3c) can be attributed to nickel oxyhydroxide (NiOOH)

Table 1
The binding energies (BEs, in eV) and the kinetic energies (KEs, in eV) of Pt-MG samples.

Sample	Pt	Cu		Ni	NiOOH	P	Phosphate(s) 2p[a] BE
	$4f_{7/2}$ BE	$2p_{3/2}$ BE	LMM KE	$2p_{3/2}$ BE	$2p_{3/2}$ BE	$2p_{3/2}$ BE	
As-cast	71.0	932.0	918.5	852.2	–	129.8	132.4
533 K	71.6	932.2	918.4	852.7	–	130.1	132.9
553 K	71.5	932.1	918.5	852.7	856.2	130.0	133.1
KOH	71.3	932.0	918.7	852.6	856.1	130.2	133.2

[a] P 2p for phosphate(s) consists of P $2p_{1/2,3/2}$; however, the two energy levels cannot be resolved.

[42,45], indicating the preferential oxidation of Ni atoms in Pt-MG during high-temperature processing and KOH exposure. Although Ni and Cu have similar affinity for oxygen, the Gibbs free energies of formation of Ni oxides (NiO, NiOOH, and $Ni(OH)_2$) are more negative than that of Cu oxides (CuO, Cu_2O) [48,49]. In addition, Cu-Pt has a more negative heat of mixing than that of Ni-Pt, resulting in higher activity coefficient of Ni in Pt-rich environment [50,51]. Therefore, the formation of Ni oxides is thermodynamically more favorable than that of Cu oxides. Phosphorus (P) is present on the surface of as-cast Pt-MG as elemental P [a poorly-resolved P 2p peak (P $2p_{3/2}$ BE = 129.8 eV, Table 1, (Fig. 3d)] [42,52] and in phosphate compound(s), as indicated by the presence of a non-resolved P 2p peak (BE = 132.4 eV, Table 1, Fig. 3d) [52–55]. No further variation in the state of P is observed after thermoplastic processing but KOH appears to dissolve P (at least on the surface), as is evidenced by the nearly complete disappearance of the P 2p peak in the spectrum of the sample treated with KOH (Fig. 3d).

The XPS studies reveal two findings about the surface chemistry of Pt-MG subjected to thermoplastic processing and KOH treatment. First, the surface chemistry of Pt-MG after thermoplastic processing at 533 K is analogous to the surface chemistry of the as-cast sample, but oxidation occurs when the processing temperature approaches the crystallization temperature (563 K). Second, Pt-MG is also oxidized by KOH exposure. In both cases, the oxidation product is NiOOH as indicated by the XPS spectra. NiOOH has a strong affinity for water because of enhanced dipole moment and the presence of unsaturated oxygen atoms, which increase the number of hydrogen bonds between the water molecules and the surface [56]. An experimental study by Chang et al. has shown that NiOOH is enriched with OH^-, which can increase water adsorption, resulting in higher wettability [57]. Therefore, increased hydrophilicity observed in Pt-MG (Fig. 1) is likely due to the formation of NiOOH during thermoplastic processing and exposing to KOH. It is apparent from these results that the surface chemistry of Pt-MG can be maintained over the course of thermoplastic processing at low temperatures. Any KOH exposure or high-temperature processing, however, results in the preferential oxidation of the Ni in Pt-MG. Similar issues are expected for MGs that are even more prone to oxidation. These changes in surface chemistry may preclude clear understanding of the correlation between topography and wetting in MGs. Therefore, the thermoplastic patterning of MGs using silicon or AAO molds is not ideal for wetting studies when KOH is required for mold separation.

3.1.1. The effect of oxidation on wetting

To understand the effect of oxidation on wetting, we used our recently developed mechanical demolding [39] to make two identical sets of Pt-MG with different topographies. To avoid oxidation and KOH exposure, both the molding and the mechanical demolding were carried out at 533 K. During molding, the MG was pressed slowly against the mold until the pressure reached 10 MPa. During demolding, the MG was pulled away at a speed of 120 mm/min. To prevent crystallization, both the molding and the demolding were completed within 60 s. After measuring the water CAs, the first set of MGs was treated with KOH for 10 min. Then the second set was annealed at 553 K for one minute. Fig. 4 shows the SEM images of the patterned Pt-MG surfaces and their wettability before and after each processing step. The water CAs of the mechanically demolded samples increased from 57° to 113° as the surface textures of these samples changed. In contrast, all of the samples exposed to KOH or annealed at 553 K exhibited hydrophilic behavior (CA ~ 15° – 47°) because of oxidation, regardless of their topographies. These results suggest that oxide formation during KOH exposure or annealing can obscure the topographic effects on the wetting of MGs, and hence, chemical demolding is not suitable in studying the correlation between the topography of MGs and their wetting behavior.

3.1.2. The effect of topography on wetting

To investigate the role of topography, Pt-MG was patterned to systematically vary the fractional solid area (f_s). To avoid KOH exposure, the samples were mechanically demolded. Fig. 5a shows the CAs of water droplets on MG surfaces with different f_s. Hydrophilic MGs initially turned hydrophobic with decreasing f_s, but they became hydrophilic again at lower f_s. This wetting behavior can be explained by the reversible Wenzel-to-Cassie wetting transition. The Cassie-Baxter model predicts that the apparent contact angle of a material can be increased even if the CA of the smooth surface of that material is less than 90° [58]. This model is thus appropriate for describing the topography-induced hydrophobicity in hydrophilic MGs observed in this study. The micro-pillars on the surface trap air in the gaps between them. This trapped air acts as a cushion, preventing water from penetrating the gaps. As a result, the wetting state changes from Wenzel to Cassie, in which the droplet sits on a heterogeneous solid-air surface (Fig. 5b). According to the Cassie-Baxter model, CA can be increased by decreasing f_s (i.e. by minimizing solid-liquid contact area) as illustrated in Fig. 5c. The experimental results did not show that CA increases monotonically as f_s decreases. Instead, we observed a decline in CA at lower f_s values (≤ 0.03). This change is due to the transition of wetting state from Cassie to Wenzel. Increasing the gap (r) between the pillars, as depicted in Fig. 5d, reduces the solid-liquid contact area and yields a higher CA. If the space between the pillars is too large, however, the liquid bridge can collapse as the water pressure overcomes the pressure of trapped air supporting it. The pressure needed to penetrate the grooves depends exclusively on the capillary pressure; because the effect of hydrostatic pressure is negligible as the radius of the droplet is smaller than the capillary length. The capillary pressure (p_c) needed to overcome the trapped air pressure and to wet the grooves depends on the spacing, however, and can be expressed as:

$$p_c = \frac{2\gamma \cos\theta}{r'}, \tag{2}$$

where r' and γ are the space between two pillars and the surface tension of the water, respectively. Since p_c is inversely proportional to r', increasing the spacing facilitates water penetration into the grooves. As a result, the wetting regime switches from Cassie to Wenzel when $f_s < 0.1$ and the CA decreases.

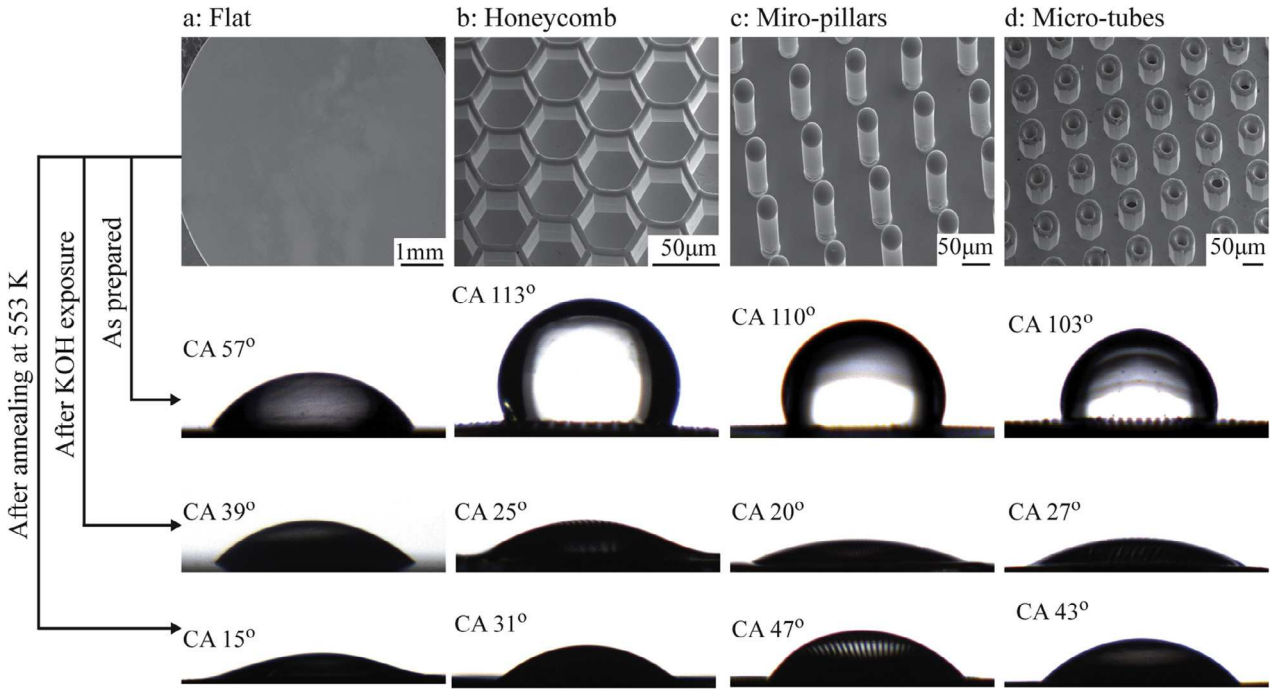

Fig. 4. The wetting behavior of flat and textured Pt-MGs at three stages: as prepared, after KOH exposure (10 min), and after annealing (553 K). The measurement error for CA was ±5°.

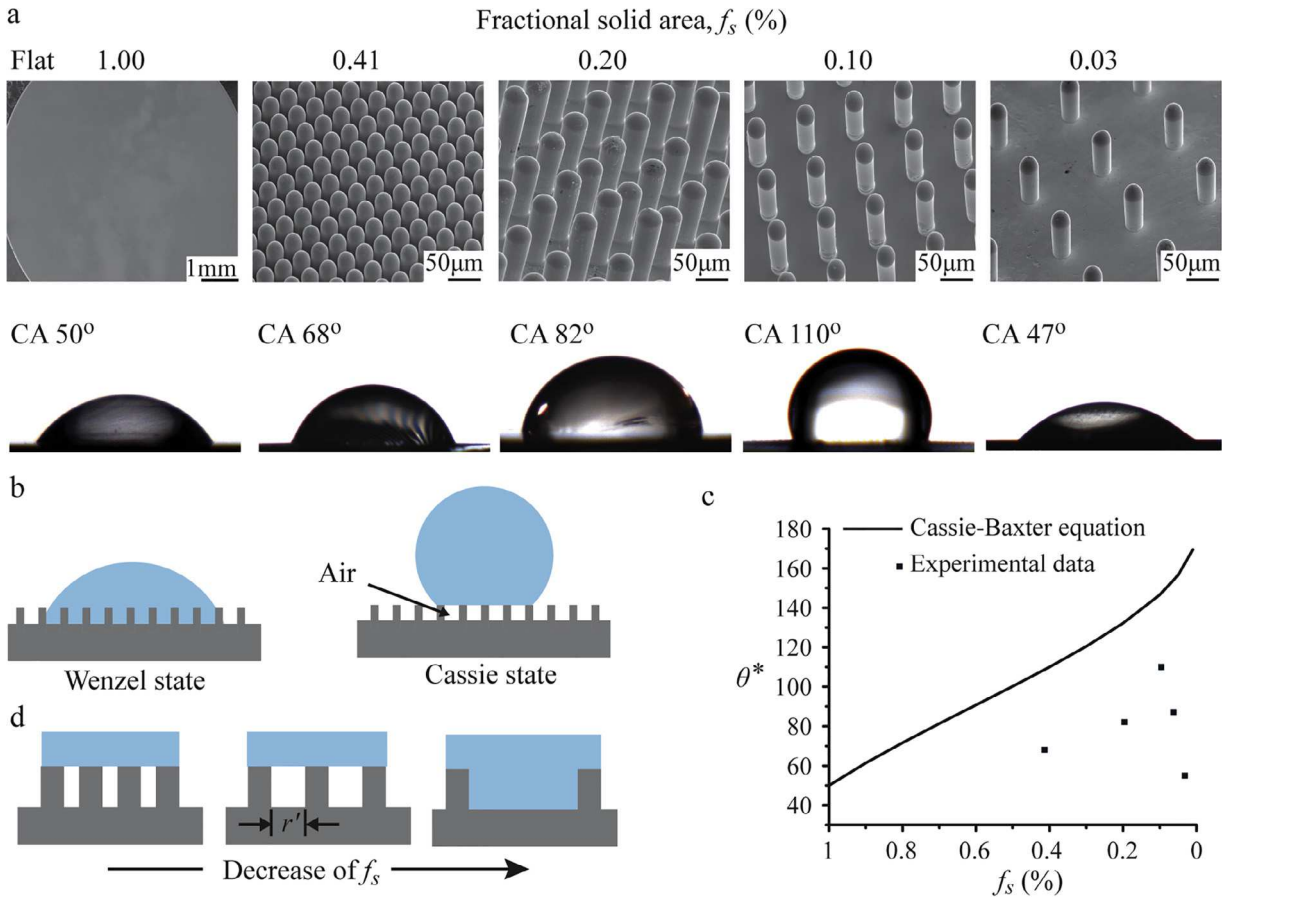

Fig. 5. Changing the wetting behavior of Pt-MG by varying the fractional solid area (f_s). (a) SEM images of flat and micro-patterned surfaces with different f_s (top row) and photographs showing the wettability of these surfaces (bottom row). The micro-pillars are equal in diameter (25 μm) and aspect ratio (3). (b) The Wenzel and the Cassie wetting states on a rough surface. (c) Comparison of the experimental CAs for different f_s to those predicted by the Cassie-Baxter equation ($\theta_Y = 50°$). (d) Schematic of the solid-liquid contact scenarios for different spacings (r') between the pillars. Larger spacings have lower f_s (and less solid-liquid contact), but pillars located too far apart cause the liquid bridge to collapse.

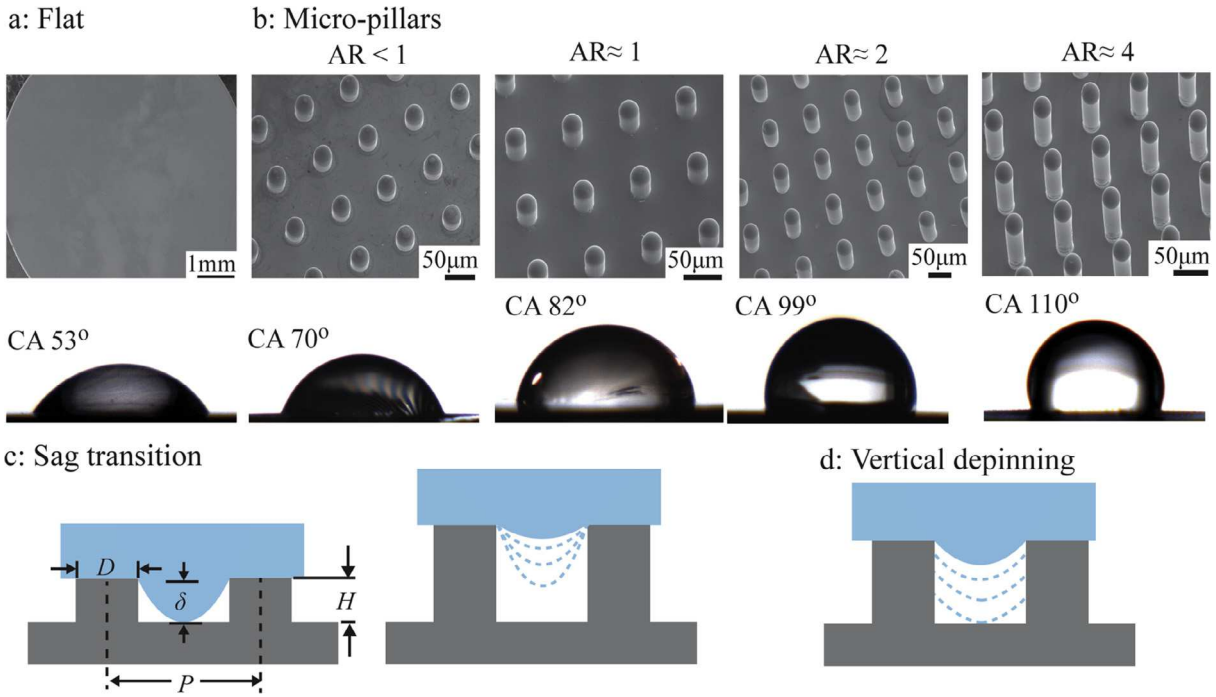

Fig. 6. The role of aspect ratio in the wetting transition. (a, b) SEM images of flat and micro-patterned Pt-MGs with four different aspect ratios (top row) and photographs showing the behavior of water droplets on these surfaces (bottom row). (c, d) Schematics for sag transition and vertical depinning, respectively.

The aspect-ratio of the surface features is also critical to stabilizing the heterogeneous wetting state, as demonstrated in Fig. 6. The two transition mechanisms [59], sag (Fig. 6c) and vertical depinning (Fig. 6d), depend on the aspect-ratio of the pillars. The liquid bridge can remain pinned at the top of the pillars but form a downward curve because of the Laplace pressure, which relates the pressure inside a drop to its curvature. The curve of a pinned droplet can touch the base when the wetting transitions to a "sag" type (this is also known as drooping). The maximum sag, or droop, (δ) of the droplet occurs directly between the two pillars and can be defined as [60]:

$$\delta \approx \frac{(\sqrt{2P} - D)^2}{8R}, \tag{3}$$

where P is the pitch between two pillars, D is the width (or diameter) of the pillars, and R is the radius of droplet curvature. The wetting state transitions from Cassie to Wenzel if $\delta \geq$ pillar height (H). High aspect-ratio structures can prevent the transition from Cassie to Wenzel, thereby preserving the hydrophobicity. If the liquid bridge cannot remain pinned at the top of the pillar, it droops downwards into the grooves and fully wets the surface of the base. As a result, the wetting becomes homogenous and the CA decreases. A lack of pinning occurs if the contact angle formed by the liquid-air interface is greater than the maximum contact angle (advancing contact angle) sustainable at the corner of the specific liquid-pillar system [61]. The roughness of the sidewalls of the pillars may hinder liquid penetration after multiple depinnings. Hence, high aspect-ratio structures can maintain the heterogeneous wetting state and high CAs despite liquid infiltration.

3.2. The wetting of Pd-MG

Mechanical demolding was also used to study the wetting behavior of $Pd_{43}Cu_{27}Ni_{10}P_{20}$ (Pd-MG). To compare the effects of topographies, Pd-MG was thermoplastically patterned with three different textures: flat, micro-pillars, and honeycomb structure. Two flat samples were made through thermoplastic forming at 613 K and 633 K. The patterned surfaces were produced by thermoplastic molding and mechanical demolding at 633 K. Fig. 7 shows the wetting behavior of the flat and the textured Pd-MG samples. Although similar patterns increased the CA of Pt-MG (Fig. 4), the CAs for the patterned Pd-MG were lower than those of the flat samples. Because Pd-MG is prone to oxidation, oxides readily form on the surface of Pd-MG within the temperature ranges required for thermoplastic embossing [Supplementary Information (SI) 1]. As a result, the CA of the flat surface prepared at 633 K was lower than that of the flat surface prepared at 613 K. When oxides accumulate, they can undermine the topographic effect and cause the Pd-MG to retain its hydrophilic nature. SI 1 provides more details on the surface oxidation and wetting behavior of the flat Pd-MG under different processing conditions. Similar hydrophilicity was also observed in the Pd-MG that was demolded chemically (see Fig. SI 1.2). As with Pt-MG, KOH alters the surface chemistry of Pd-MG, influencing its wettability. Our results contradict those of previous studies, showing the hydrophobicity of textured Pd-based MGs demolded via chemical etching [29,31]. However, we did observe time-dependent superhydrophobicity

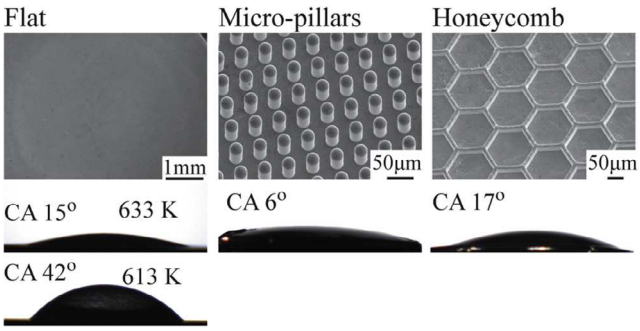

Fig. 7. SEM images of flat, micro-pillar, and honeycomb Pd-MGs (top row) and photograph showing the wettability of those surfaces (bottom rows).

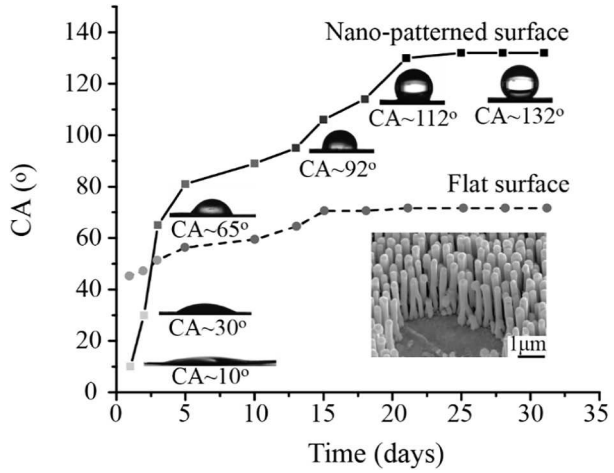

Fig. 8. The wetting kinetics of flat and nano-patterned Pd-MGs. (Inset) An SEM image of a nano-patterned Pd-MG.

in patterned Pd-MG. Fig. 8 demonstrates the wetting kinetics of chemically demolded Pd-MG. Flat Pd-MG remained hydrophilic regardless of the time between sample preparation and CA measurement, while nano-textured Pd-MG became superhydrophobic after ten days in air. The time dependence of superhydrophilicity can also be correlated with the surface chemistry changes in the air. Previous studies hypothesized that increase in the carbon adsorption on metallic surfaces could cause this time-dependent superhydrophobicity [15,62,63]. To verify this hypothesis, we quantified the chemical composition of the nano-patterned Pd-MG surface at day 1 and at day 20 and compared the results to the carbon content of the flat surface. The XPS results show that the nano-patterned surface adsorbed more carbon than did the flat surface (Fig. 9). The atomic percentage of carbon of the flat Pd-MG surface increased by 7%, while the carbon content of the nano-patterned Pd-MG surface increased by 14%. This increase in carbon adsorption can be attributed to the large surface area of MG nanostructures. Spontaneous deposition of hydrocarbon molecules on nano-textured surfaces has also been reported in other nanostructured materials [62–64]. Time-dependent wetting transitions were also observed in the mechanically demolded samples (see SI 2).

4. Conclusions

By decoupling the chemical effects, this study demonstrates the effect of topography on the wetting of Pt-MG. We used thermoplastic embossing to texture the surface of MG. Our early observations revealed that Pt-MG is prone to oxidation in its supercooled liquid state and during chemical demolding. To prevent the oxidation, we optimized the thermoplastic embossing temperature for Pt-MG and used chemical-free demolding. This surface texturing protocol allowed us to pattern the Pt-MG systematically without affecting its chemical and structural states and thus to decouple the topographic and chemical effects on wetting. Our wetting experiments show that inherently hydrophilic Pt-MG can be

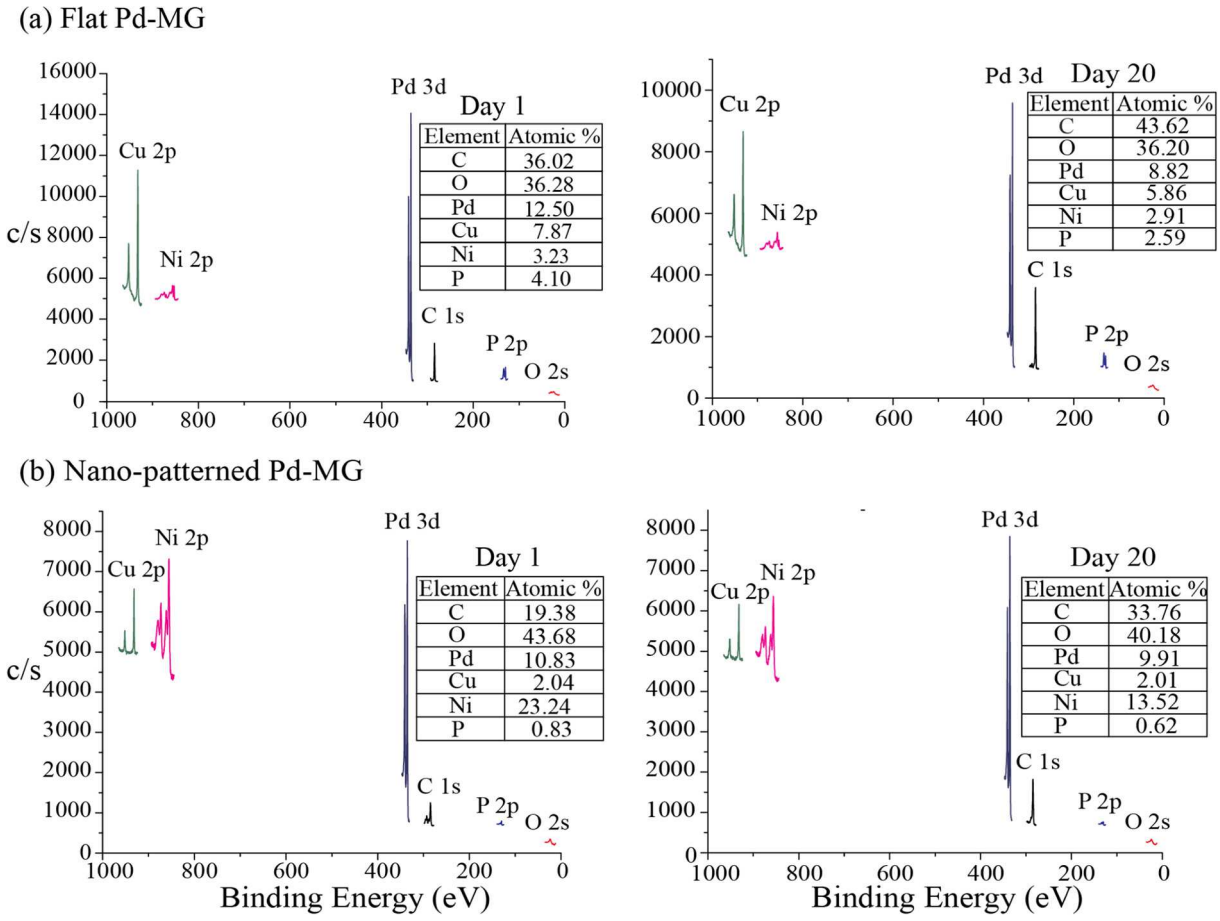

Fig. 9. The XPS spectra and atomic percentages of Carbon (C), Oxygen (O), Palladium (Pd), Copper (Cu), Nickel (Ni), and Phosphorous (P) for (a) a flat Pd-MG and (b) a nano-patterned Pd-MG.

rendered hydrophobic through topographic controls (e.g. through the embossing of single-scale micro-patterns). Previous studies have shown that Pd-based MGs demolded via chemical etching can exhibit hydrophobicity but our findings contradict this. Both of the MGs studied here (Pt- and Pd-MG) remained hydrophilic after chemical demolding regardless of their topographies. Moreover, because Pd-MG is prone to oxidation at high processing temperatures, even mechanical demolding cannot prohibit concomitant changes in surface chemistry during texturing. As a result, the patterned Pd-MG did not show any wetting transition. We did notice, however, that the wetting of Pd-MG is highly sensitive to time. Preliminary XPS data suggest the adsorption of carbon as a possible reason for this time dependence. However, a systematic study of Pd-MG is needed to reconcile our data with that of the published literature. Furthermore, understanding the effect of carbon adsorption on other MGs is necessary to ascertain carbon's role in the time-dependent transition from hydrophilic to hydrophobic.

Acknowledgement

This work was supported by National Science Foundation through CAREER Award #CMMI-1653938. The SEM characterization was conducted using Hitachi S-4300 acquired through NSF Major Research Instrumentation Program Award #0421032.

Appendix A. Supplementary material

Supplementary data associated with this article can be found, in the online version, at https://doi.org/10.1016/j.apsusc.2018.03.205.

References

[1] E. Hermelin, J. Petitjean, J.C. Lacroix, K.I. Chane-Ching, J. Tanguy, P.C. Lacaze, Chem. Mater. 20 (2008) 4447–4456.
[2] J. Bravo, L. Zhai, Z. Wu, R.E. Cohen, M.F. Rubner, Langmuir 23 (2007) 7293–7298.
[3] W.L. Min, B. Jiang, P. Jiang, Adv. Mater. 20 (2008) 3914–3918.
[4] L. Cao, A.K. Jones, V.K. Sikka, J. Wu, D. Gao, Langmuir 25 (2009) 12444–12448.
[5] A.K. Kota, G. Kwon, W. Choi, J.M. Mabry, A. Tuteja, Nat. Commun. 3 (2012) 1025.
[6] F. Shi, J. Niu, J. Liu, F. Liu, Z. Wang, X.Q. Feng, X. Zhang, Adv. Mater. 19 (2007) 2257–2261.
[7] J.G. Fan, X.J. Tang, Y.P. Zhao, Nanotechnology 15 (2004) 501–504.
[8] B. Bhushan, Y.C. Jung, K. Koch, Langmuir 25 (2009) 3240–3248.
[9] F. Rupp, L. Scheideler, D. Rehbein, D. Axmann, J. Geis-Gerstorfer, Biomaterials 25 (2004) 1429–1438.
[10] J. Bico, C. Tordeux, D. Quere, Europhys. Lett. 55 (2001) 214–220.
[11] A. Sabbah, A. Youssef, P. Damman, Appl. Sci. 6 (2016) 152.
[12] B. Bhushan, Y.C. Jung, K. Koch, Phil. Trans. Royal Soc. A 367 (2009) 1631–1672.
[13] E. Hosono, H. Matsuda, I. Honma, M. Ichihara, H. Zhou, Langmuir 23 (2007) 7447–7450.
[14] P. Bhattacharya, S. Gohil, J. Mazher, S. Ghosh, P. Ayyub, Nanotechnology 19 (2008) 075709.
[15] A.M. Kietzig, S.G. Hatzikiriakos, P. Englezos, Langmuir 25 (2009) 4821–4827.
[16] A.Y. Vorobyev, C. Guo, J. Appl. Phys. 117 (2015) 033103.
[17] A.M. Kietzig, M.N. Mirvakili, S. Kamal, P. Englezos, S.G. Hatzikiriakos, J. Adhes. Sci. Technol. 25 (2011) 2789–2809.
[18] E. Bormashenko, T. Stein, G. Whyman, Y. Bormashenko, R. Pogreb, Langmuir 22 (2006) 9982–9985.
[19] Y. Saotome, T. Zhang, A. Inoue, Mat. Res. Soc. Symp. Proc. 554 (1999) 385–390.
[20] A.Y. Vorobyev, C. Guo, Laser Photonics Rev. 7 (2013) 385–407.
[21] J.T. Han, Y. Jang, D.Y. Lee, J.H. Park, S.H. Song, D.Y. Ban, K. Cho, J. Mater. Chem. 15 (2005) 3089–3092.
[22] Z. Chen, Y. Guo, S. Fang, Surf. Interface Anal. 42 (2010) 1–6.
[23] Z. Guo, J. Liang, J. Fang, B. Guo, W. Liu, Adv. Eng. Mater. 9 (2007) 316–321.
[24] A.L. Greer, Science 267 (1995) 1947–1953.
[25] W.L. Johnson, MRS Bull. 24 (1999) 42–56.
[26] G. Kumar, H.X. Tang, J. Schroers, Nature 457 (2009) 868–872.
[27] M. Hasan, J. Schroers, G. Kumar, Nano Lett. 15 (2015) 963–968.
[28] J. Schroers, JOM 57 (2005) 35–39.
[29] T. Xia, N. Li, Y. Wu, L. Liu, Appl. Phys. Lett. 101 (2012) 081601.
[30] N. Li, T. Xia, L. Heng, L. Liu, Appl. Phys. Lett. 102 (2013) 251603.
[31] H.S. Arora, Q. Xu, Z. Xia, Y.H. Ho, N.B. Dahotre, J. Schroers, S. Mukherjee, Scripta Mater. 69 (2013) 732–735.
[32] K. Zhao, K.S. Liu, J.F. Li, W.H. Wang, L. Jiang, Scripta Mater. 60 (2009) 225–227.
[33] K. Liu, Z. Li, W. Wang, L. Jiang, Appl. Phys. Lett. 99 (2011) 261905.
[34] M. Gao, D.P. Wang, Y.F. Huang, S. Meng, W.H. Wang, Mater. Des. 95 (2016) 612–617.
[35] H. Huang, J. Yan, J. Micromech. Microeng. 27 (2017) 075007.
[36] J. Schroers, Adv. Mater. 22 (2010) 1566–1597.
[37] N. Li, W. Chen, L. Liu, JOM 68 (2016) 1246–1261.
[38] S. Ding, J. Kong, J. Schroers, J. Appl. Phys. 110 (2011) 043508.
[39] M. Hasan, G. Kumar, Scripta Mater. 123 (2016) 140–143.
[40] R.N. Wenzel, J. Phys. Chem. 53 (1949) 1466–1467.
[41] K.S. Kim, N. Winograd, R.E. Davis, J. Am. Chem. Soc. 93 (1971) 6296–6297.
[42] J.F. Moulder, W.F. Stickle, P.E. Sobol, K.D. Bomben, Handbook of X-ray Photoelectron Spectroscopy, Perkin-Elmer Corporation, 1992.
[43] G. Schon, Surf. Sci. 35 (1973) 96–108.
[44] G. Deroubaix, P. Marcus, Surf. Interf. Anal. 18 (1992) 39–46.
[45] A.P. Grosvenor, M.C. Biesinger, R.S.C. Smart, N.S. McIntyre, Surf. Sci. 600 (2006) 1771–1779.
[46] https://xpssimplified.com/elements/nickel.php.
[47] M.C. Biesinger, B.P. Payne, L.W.M. Lau, A. Gerson, R.S.C. Smart, Surf. Interface Anal. 41 (2009) 324–332.
[48] J.A. Dean, Lange's Handbook of Chemistry, 15th ed., McGraw-Hill, Inc., 1998.
[49] H. Gamsjager, J. Bugajski, T. Gadja, R.J. Lemire, W. Preis, Chemical Thermodynamics of Nickel, Elsevier, 2005.
[50] L.R. Bidwell, W.J. Schulz, R.K. Saxer, Acta Metall. 15 (1967) 1143–1151.
[51] F. Lantelme, A. Salmi, J. Phys. Chem. 100 (1996) 1159–1163.
[52] http://xpssimplified.com/elements/phosphorus.php.
[53] http://www.xpsfitting.com/2013/01/phosphorus.html.
[54] R. Gopalakrishnan, B.V.R. Chowdari, K.L. Tan, Mater. Res. Bull. 26 (1991) 1371–1378.
[55] B.V.R. Chowdari, K.L. Tan, W.T. Chia, R. Gopalakrishnan, Solid State Ionics 40–41 (1990) 684–688.
[56] M.J. Eslamibidgoli, A. Gross, M. Eikerling, Phys. Chem. Chem. Phys. 19 (2017) 22659–22669.
[57] Y.H. Chang, N.Y. Hau, C. Liu, Y.T. Huang, C.C. Li, K. Shih, S.P. Feng, Nanoscale 6 (2014) 15309–15315.
[58] A.B.D. Cassie, S. Baxter, Trans. Faraday Soc. 40 (1944) 546–551.
[59] N.A. Patankar, Langmuir 26 (2010) 8941–8945.
[60] Y.C. Jung, B. Bhushan, Scripta Mater. 57 (2007) 1057–1060.
[61] N.A. Patankar, Langmuir 20 (2004) 7097–7102.
[62] S. Khorsand, K. Raeissi, F. Ashrafizadeh, M.A. Arenas, Chem. Eng. J. 273 (2015) 638–646.
[63] L.B. Boinovich, A.M. Emelyanenko, A.S. Pashinin, C.H. Lee, J. Drelich, Y.K. Yap, Langmuir 28 (2012) 1206–1216.
[64] M.R.S. Shirazy, S. Blais, L.G. Frechette, Appl. Surf. Sci. 258 (2012) 6416–6424.